Electron Dynamics in Hybrid Perovskites Reveal the Role of Organic Cations on the Screening of Local Charges

Marie Cherasse, Jingwei Dong, Gaëlle Trippé-Allard, Emmanuelle Deleporte, Damien Garrot, Sebastian Maehrlein, Martin Wolf, Zhesheng Chen, Evangelos Papalazarou, Marino Marsi, et al.

Electron dynamics in hybrid perovskites reveal the role of organic cations on the screening of local charges

Marie Cherasse,[†,‡] Jingwei Dong,[*,†] Gaëlle Trippé-Allard,[¶] Emmanuelle Deleporte,[¶] Damien Garrot,[§] Sebastian F. Maehrlein,[‡] Martin Wolf,[‡] Zhesheng Chen,[‖] Evangelos Papalazarou,[⊥] Marino Marsi,[⊥] Jean-Pascal Rueff,[#,@] Amina Taleb-Ibrahimi,[#] and Luca Perfetti[*,†]

†*Laboratoire des Solides Irradiés, CEA/DRF/lRAMIS, CNRS, Ecole Polytechnique, Institut Polytechnique de Paris, 91128 Palaiseau, France*

‡*Fritz Haber Institute of the Max Planck Society, Faradayweg 4-6, 14195 Berlin, Germany*

¶*Université Paris-Saclay, ENS Paris-Saclay, CentraleSupélec, CNRS, LuMIn, F-91190 Gif-sur-Yvette, France*

§*Université Paris-Saclay, UVSQ, CNRS, GEMaC, F-78000 Versailles, France*

‖*Laboratoire de Physique des Solidés, Université Paris-Saclay, CNRS, 91405 Orsay, France*

⊥*Laboratoire de Physique des Solides, Université Paris-Saclay, CNRS, 91405 Orsay, France*

#*Synchrotron SOLEIL, L'Orme des Merisiers, Saint-Aubin - BP 48, 91192 Gif-sur-Yvette, France*

@*Sorbonne Université, CNRS, Laboratoire de Chimie Physique-Matière et Rayonnement, F-75005 Paris, France*

E-mail: djw1991@dicp.ac.cn; luca.perfetti@polytechnique.edu

Abstract

The large tolerance of hybrid perovksites to the trapping of electrons by defects is a key asset in photovoltaic applications. Here, the ionic surface terminations of $CH_3NH_3PbI_3$ are employed as testbed to study the effect of electrostatic fields on the dynamics of excited carriers. We characterize the transition across the tetragonal to orthorhombic phase. The observed type II band offset and drift of the excited electrons highlight the important role that organic cations have on the screening of local electrostatic fields. When the orientation of organic cations is frozen in the orthorhombic phase, the positively charged termination induces a massive accumulation of excited electrons at the surface of the sample. Conversely, no electron accumulation is observed in the tetragonal phase. We conclude that the local fields cannot penetrate in the sample when the polarizability of freely moving cations boosts the dielectric constant up to $\varepsilon = 120$.

Keywords: Hybrid Perovskites, time resolved spectroscopy, band alignment, screening.

Introduction

Metal halide perovskites are attracting widespread interest because of their excellent performance in photovoltaic devices and optoelectronic applications. As for any other semiconductor, the transport and photovoltaic properties of these compounds can be influenced by disorder and impurities. However, the excellent tolerance to defect scattering in metal halide perovskites is the subject of considerable debate.[1–3] Indeed, the high charge-collection efficiencies and open-circuit voltage of the derived solar cells suggest that both the carriers recombination rate and trapping rates are particularly low.[4] On the other hand, the active layer is usually a polycrystalline thin film, where grain boundaries could create a large amount of trapping centers. Several authors have connected the exceptional electronic properties of metal halide perovskites to the polarizability of the nuclear lattice.[5–7] The complex permittivity experiments on the tetragonal phase of $CH_3NH_3PbI_3$ have shown that collective

reorientations of organic cations result in a dielectric constant attaining values larger than 120 below 1 GHz.[5,8] This massive dipole relaxation around trapping centers has no analogous in conventional semiconductors. It follows that any carrier approaching a charged defect will not be affected, unless coming closer than two unit cells.[5] The defect tolerance due to large dielectric screening prevails in the tetragonal phase of $CH_3NH_3PbI_3$ where the orientation of organic dipoles can be very easily switched. Instead, upon crossing the tetragonal to orthorhombic phase transition, the organic moiety freezes in an ordered structure, leading to a sudden drop of the dielectric function from 120 to 30.[5,8] In this case, the electrostatic field generated by charged traps and polar interfaces should make a visible impact on the dynamics of photo-carriers. To the best of our knowledge, the evidence of this forecast has so far remained elusive.

In this work, we design an experiment investigating if the organic cations are capable of efficiently screen charged defects or polar interfaces. The surface of $CH_3NH_3PbI_3$ displays indeed two possible terminations, the zigzag and dimerized one, both featuring a net positive charge of $\cong 0.25e^+$ in the topmost CH_3NH_3-I layer.[9] The net charges on the CH_3NH_3-I and Pb-I_2 layers are alternatively positive and negative, implying the build up of a domain with permanent dipole moments perpendicular to the surface.[10] This process is general to any ionic termination and in the case of $CH_3NH_3PbI_3$ may play a role in the hysteretic behavior of $I-V$ curves.[11] If capable of penetrating sufficiently in the crystal, the local electrostatic potential generated by the charged terminations would induce an accumulation of photoexcited electrons at the surface. In order to test this conjecture, we combine one photon and two photon photoemission experiments to access the energy of electronic states and ultrafast dynamics of excited carriers. Due to the short escape depth of photoelectrons, the probed region is within 3-5 nanometers from the surface.[12] By performing temperature dependent measurements, we reveal the band offset between the orthogonal and orthorhombic phase of $CH_3NH_3PbI_3$. Moreover, we find that the electrostatic potential of the charged surface is fully screened in the tetragonal phase but drastically modifies the electron dynamics in the

orthorhombic phase.

Data and analysis

Single crystals of $CH_3NH_3PbI_3$ have been grown by inverse temperature crystallization method. Methylammonium iodide (0.78 g, 5 mmol) and lead iodide (2.30 g, 5 mmol) were dissolved in gamma-butyrolactone (5 mL) at 60 °C. The yellow solution (2 mL) was placed in a vial and heated at 120 °C during one to four hours depending on the desired crystal size. The high quality of the single crystals is verified by X-ray diffraction measurements of Bragg's reflections. Despite the high crystalline quality of our samples, Low Energy Electron Diffraction (LEED) did not display the Bragg spots.[13] Moreover, the electronic bands did not feature the dispersion that has been reported in epitaxially grown films.[13–15] We evince that cleaved surfaces are rough, probably because of the brittle nature of $CH_3NH_3PbI_3$. For photoemission measurements, the single crystal have been cleaved at the base pressure of 10^{-10} mbar and temperature of 180 K. It is essential to cleave the crystal cold in order to ensure that no sublimation of organic cations could alter the surface stoichiometry.

Figure 1 shows Hard X-ray PhotoElectron Spectroscopy (HAXPES) measurements of $CH_3NH_3PbI_3$ at temperature of 180 K (tetragonal phase) and 120 K (orthorhombic phase), performed at the GALAXIES beamline of SOLEIL synchrotron.[16] The spectra have been acquired within a total accumulation time shorter than few minutes, in order to minimize sample degradation to the exposure of 3 keV photons. Both the core levels and valence band display a rigid shift towards lower energy when the system is in the low symmetry phase (120 K). The lack of any other appreciable change in the spectral shape indicates that the electronic density of states and atomic valences are almost unaffected by the structural transition.

A combination of direct photoemission and two photon photoemission (2PPE) is employed in order to follow the bands offset as a function of temperature.[17] Our photon source

is a Ti:sapphire laser system delivering 6 μJ pulses with a repetition rate of 250 kHz. The fundamental beam (1.55 eV) is partially converted into a second harmonic (3.15 eV), third harmonic (4.7 eV) and fourth harmonic (6.3 eV) beam. We make use of the latter in order to monitor photoelectrons from the valence band maximum (VBM). Instead, 2PPE with 3.15 eV pump and 4.7 eV probe are employed to transiently populate and subsequently probe the energy of the Conduction Band Minimum (CBM). The pump beam is absorbed in a penetration depth of 50 nm and generates an electron density of 5×10^{18} cm^{-3}.

The upper panel of Fig. 2A shows the pump-on minus pump-off signal resulting from the 2PPE process. We have set the delay between the two beams to 1.5 picosecond, which is much larger than the typical cooling time of hot carriers.[18] The kinetic energy position of the chemical potential is obtained from the Fermi level of a copper reference that is in Ohmic contact with the sample. For the sake of simplicity, we do not plot the data with respect to kinetic energy, but with respect to a rescaled energy axis where the chemical potential is set to zero. Roughly 0.4 eV above the chemical potential, a peak in the photocurrent intensity originates from electrons that have relaxed near to the CBM. This signal becomes brighter and shifts by -0.1 eV when the sample is cooled below the phase transition temperature of 159 K. The lowering of CBM energy indicates that the positively charged surface terminations are less screened in the orthorhombic phase than in the tetragonal one. Accordingly, the higher photocurrent intensity that can be observed below the transition temperature is due to the electron accumulation provoked by a local electrostatic potential.

Note also that, near to zero energy, a second peak in 2PPE intensity nearly follows the temperature evolution of the CBM. This feature is a Secondary Electron Replica (SER) ending sharply at the spectral cutoff,[4] and corresponds to photoelectrons having zero kinetic energy. The energy distance between CBM and SER is $\xi = 0.4$ eV in our crystal but depends on the stoichiometry and can shrink down to 0.1 eV in surfaces with deficiency of organic cations[18] (and that have not been cleaved cold). From these measurements we can extract the energy separation between the vacuum level and VBM, also known as Ionisation Energy

(IE). The value $IE = 5.9$ eV is derived by adding the band gap (1.6 eV) and subtracting ξ (0.4 eV) to the probe photon energy (4.7 eV). According to Emara *et al.* the IE near to 6 eV indicates that our sample has nominal stoichiometry.[19]

The lower panel of Fig. 2A plots a direct photoemission map of the valence band as a function of temperature. The VBM (marked by a dashed white line) is identified by the threshold where the photocurrent intensity drops below the noise level. By lowering the temperature below 159 K, the VBM shifts by -0.2 eV, in agreement with the results obtained via HAXPES and that have been shown in Fig 1. Two white arrows indicate the energy distance between CBM and VBM, either below or above the structural phase transition. The estimated size of the electronic gap is 1.58 eV in the tetragonal phase and 1.67 eV in the orthorhombic one, consistently with scanning tunneling spectroscopy.[9] Comparable transition temperature and gap's magnitude have been also obtained from the temperature dependent photoluminescence of Fig. 2C, therefore backing our analysis of photoelectrons intensity maps. The blue shift of bandgap in the orthorhombic phase is related to the tilting of PbI_3 octahedra and freezing of organic cations into an ordered structure (see also sketch in Fig. 2B). One of the most relevant results of this work is the type II band offset in Fig. 2A, implying that a mixed phase of $CH_3NH_3PbI_3$ would favor the separation of charge carriers, with electrons accumulating in orthorhombic structure and holes in the tetragonal one. Accordingly, photoexcited thin films of $CH_3NH_3PbI_3$ display photoluminescence from recombination of the electron-holes trapped at the domain boundary of tetragonal inclusions in the orthorhombic phase.[20] This property is probably detrimental in the context of solar energy harvesting, since active traps reduce the carriers mobility.

Next we investigate the carriers dynamics when changing the temperature across the phase transition. In the tetragonal structure, the large dielectric constant $\varepsilon = 120$ ensures that charged surface terminations are efficiently screened by the polarization of organic cations. Since a local electrostatic potential cannot build up, the bands are flat near the surface (see sketch in Fig. 3c). Photoexcited electrons follow the dynamics shown in Fig.

3, dissipating most of their excess energy by phonon emission.[14,18] At pump probe delays larger than 500 fs, the electrons are fully thermalized. Their concentration is monitored in Fig. 3b, which plots the 2PPE intensity integrated in a small energy interval centered at the CBM. This signal decays on a nanosecond timescale, mainly due to recombination with holes in the VBM or due to diffusion into the bulk of the sample, out of the probing region of the photoelectrons escape depth.[18]

The second major outcome of this work deals with the evolution of carriers dynamics when the temperature is changed across the phase transition. Indeed, the build up and relaxation of electronic signal is notably different if the crystal is in the orthorhombic structure instead of the tetragonal one (see Fig. 4A). Although the band dispersion[21] and spectral density (see Fig. 1) depend weakly on crystal symmetry, the organic cations lock in specific orientations below the transition temperature, therefore freezing their orientational degrees of freedom. Since the screening efficiency of the cations is severely compromised, the dielectric constant of the orthorhombic phase drops to $\varepsilon = 30$. Positively charged terminations can now induce a surface potential that bends the bands downward with respect to the bulk reference. The built-in field attracts electrons at the surface (sketched in Fig. 4C), leading to an increase of their local concentration with the respect to the tetragonal phase. In agreement with this picture, Fig. 2A displays downward band offset and a fourfold increase of the 2PPE signal below the transition temperature. We recall that a comparable accumulation of photoexcited electrons has been reported in the edge states of topological insulators[22] and can be viewed as a hallmark of local fields near to the sample surface. In the present case, the 2PPE intensity at the CBM of orthorhombic $CH_3NH_3PbI_3$ shows that the density of excited electrons saturates at the edge of the sample roughly 2-3 ps after photoexcitation (see Fig. 4B). Subsequently, the accumulated electrons get trapped by vacancies or interstitial defects, which generally abound on ionic surfaces. This localization explains the decay of 2PPE intensity on a timescale of 60 ps, which is visible in Fig. 4B and sketched in Fig. 4C. Indeed, strongly localized states induce a signal equally distributed at all wavevectors and

below the CBM, most of which escapes from our detection window. After 200 ps, the CBM intensity follows the nanosecond decay that has been also reported for the tetragonal phase. Being the latter a slow process, we evince that traps do not act as recombination centers but they are neutralized once filled by electrons.

Conclusions

In conclusion, the present experiment provides novel insights on the defect tolerance of $CH_3NH_3PbI_3$. We make use of ionic surface terminations as a test ground of charged defects and interfaces. The electron dynamics is measured as a function of temperature, across the tetragonal to orthorhombic phase transition. Both the bands alignment and electron dynamics indicates that electrostatic fields are strongly screened only in tetragonal phase, namely when organic cations hold an exceptionally large polarizability. Our results explain the modest impact that defects and grain boundaries have on the performances of solar cells based on hybrid perovskites. The exceptional properties of these promising compounds are indeed linked to interpenetration of highly polarizable organic cations with a rigid inorganic structure. While solar photons generate light carriers in the PbI_3^- bands, the $CH_3NH_3^+$ molecules favor the mobility by reducing the trapping rate.

Acknowledgement

We acknowledge financial support to the 2D-HYPE project from the Agence Nationale de la Recherche (ANR, Nr. ANR-21-CE30-0059), the Deutsche Forschungsgemeinschaft (DFG, German Research Foundation, Nr. 490867834) the DAAD Scholarship 57507869, and the SOLEIL Synchrotron for the provision of the beamtime (proposal 20181832). Valerie Veniard, Paolo Umari, Antonio Tejeda and Catherine Corbel contributed to the data interpretation with enlightening discussions.

References

(1) Steirer, K. X.; Schulz, P.; Teeter, G.; Stevanovic, V.; Yang, M.; Zhu, K.; Berry, J. J. Defect Tolerance in Methylammonium Lead Triiodide Perovskite. *ACS Energy Lett.* **2016**, *1*, 360.

(2) Huang, J.; Yuan, Y.; Shao, Y.; Yan, Y. Understanding the physical properties of hybrid perovskites for photovoltaic applications. *Nature Review Materials* **2017**, *2*, 17042.

(3) Knight, A. J.; Patel, J. B.; Snaith, H. J.; Johnston, M. B.; Herz, L. M. Trap States, Electric Fields, and Phase Segregation in Mixed-Halide Perovskite Photovoltaic Devices. *Adv. Energy Mater.* **2020**, *10*, 1903.

(4) Jung, E. et al. Femto-to Microsecond Dynamics of Excited Electrons in a Quadruple Cation Perovskite. *ACS Energy Lett.* **2020**, *5*, 785.

(5) Anusca, I.; Balciunas, S.; Gemeiner, P.; Svirskas, S.; Sanlialp, M.; Lackner, G.; Fettkenhauer, C.; Belovickis, J.; Samulionis, V.; Ivanov, M.; Dkhil, B.; Banys, J.; Shvartsman, V. V.; Lupascu, D. C. Dielectric Response: Answer to Many Questions in the Methylammonium Lead Halide Solar Cell Absorbers. *Advanced Energy Materials* **2015**, *106*, 221104.

(6) Tan, H. et al. Dipolar cations confer defect tolerance in wide-bandgap metal halide perovskites. *Nature Comm.* **2018**, *9*, 3100.

(7) Maehrlein, S. F.; Joshi, P.; Huber, L.; Wang, F.; Cherasse, M.; Liu, Y.; Juraschek, D. M.; Mosconi, E.; Meggiolaro, D.; De Angelis, F.; Y., Z. X. Decoding ultrafast polarization responses in lead halide perovskites by the two-dimensional optical Kerr effect. *Proc. Natl. Acad. Sci. U.S.A.* **2021**, *118*, e2022268118.

(8) Onda-Yamamuro, N.; Matsuo, T.; Suga, H. Dielectric study of $CH_3NH_3PbX_3$ (X = Cl, Br, I). *J. Phys. Chem. Solids* **1992**, *53*, 935.

(9) She, L.; Liu, M.; Zhong, D. Atomic Structures of $CH_3NH_3PbI_3$ (001) Surfaces. *ACS Nano* **2016**, *10*, 1126.

(10) Seidu, A.; Dvorak, M.; Järvi, J.; Rinke, P.; Li, J. Surface reconstruction of tetragonal methylammonium lead triiodide. *APL Mater.* **2021**, *9*, 111102.

(11) Caddeo, C.; Filippetti, A.; Mattoni, A. The dominant role of surfaces in the hysteretic behavior of hybrid perovskites. *Nano Energy* **2020**, *67*, 104162.

(12) Chen, Z.; Dong, J.; Giorgetti, G.; Papalazarou, E.; Marsi, M.; Zhang, Z.; Tian, B.; Ma, Q.; Cheng, Y.; Rueff, J.-P.; Taleb-Ibrahimi, A.; Perfetti, L. Spectroscopy of buried states in black phosphorus with surface doping. *2D Materials* **2020**, *7*, 035027.

(13) Yang, J.-P.; Meissner, M.; Yamaguchi, T.; Zhang, X.-Y.; Ueba, T.; Cheng, L.-W.; Ideta, S.; Tanaka, K.; Zeng, X.-H.; Ueno, N.; Kera, S. Spectroscopy of buried states in black phosphorus with surface doping. *Sol. RRL* **2018**, *2*, 1800132.

(14) Niesner, D.; Zhu, H.; Miyata, K.; Joshi, P. P.; Evans, T. J. S.; Kudisch, B. J.; Trinh, M. T.; Marks, M.; Zhu, X.-Y. Persistent Energetic Electrons in Methylammonium Lead Iodide Perovskite Thin Films. *J. Am. Chem. Soc.* **2016**, *138*, 15717.

(15) Niesner, D. Surface electronic structure and dynamics of lead halide perovskites. *APL Mater.* **2020**, *8*, 090704.

(16) Rueff, J.-P.; Ablett, J. M.; Céolin, D.; Prieur, D.; Moreno, T.; Baldédent, V.; Lassalle, B.; Rault, J. E.; Simon, M.; Shukla, A. The GALAXIES Beamline at SOLEIL Synchrotron: Inelastic X-ray Scattering and Photoelectron Spectroscopy in the Hard X-ray Range. *J. Synchrotron Rad.* **2015**, *22*, 175.

(17) Faure, J.; Mauchain, J.; Papalazarou, E.; Yan, W.; Pinon, J.; Marsi, M.; Perfetti, L. Full characterization and optimization of a femtosecond ultraviolet laser source for time and angle-resolved photoemission on solid surfaces. *Rev. Sci. Instrum.* **2012**, *83*, 043109.

(18) Chen, Z.; Lee, M. I.; Zhang, Z.; Diab, H.; Garrot, D.; Ledee, F.; Fertey, P.; Papalazarou, E.; Marsi, M.; Ponseca, C.; Deleporte, E.; Tejeda, A.; Perfetti, L. Time-Resolved Photoemission Spectroscopy of Electronic Cooling and Localization in $CH_3NH_3PbI_3$ Crystals. *Phys. Rev. Mater.* **2017**, *1*, 045402.

(19) Emara, J.; Schnier, T.; Pourdavoud, N.; Riedl, T.; Meerholz, K.; Olthof, S. Impact of Film Stoichiometry on the Ionization Energy and Electronic Structure of $CH_3NH_3PbI_3$. *Adv. Mater.* **2016**, *28*, 553.

(20) Diab, H.; Trippé-Allard, G.; Lédée, F.; Jemli, K.; Vilar, C.; Bouchez, G.; Jacques, V. L. R.; Tejeda, A.; Even, J.; Lauret, J.-S.; Deleporte, E.; Garrot, D. Narrow Linewidth Excitonic Emission in Organic Inorganic Lead Iodide Perovskite Single Crystals. *J. Phys. Chem. Lett.* **2016**, *7*, 5093.

(21) Wang, Y.; Zhang, Y.; P., Z.; Zhang, W. High intrinsic carrier mobility and photon absorption in the perovskite $CH_3NH_3PbI_3$. *Phys. Chem. Chem. Phys.* **2015**, *17*, 11516.

(22) Papalazarou, E.; Khalil, L.; Caputo, M.; Perfetti, L.; Nilforoushan, N.; Deng, H.; Chen, Z.; Zhao, S.; Taleb-Ibrahimi, A.; Konczykowski, M.; Hruban, A.; Wolos, A.; Materna, A.; Krusin-Elbaum, L.; Marsi, M. Unraveling the Dirac fermion dynamics of the bulk-insulating topological system Bi_2Te_2Se. *Phys. Rev. Mater.* **2018**, *2*, 104202.

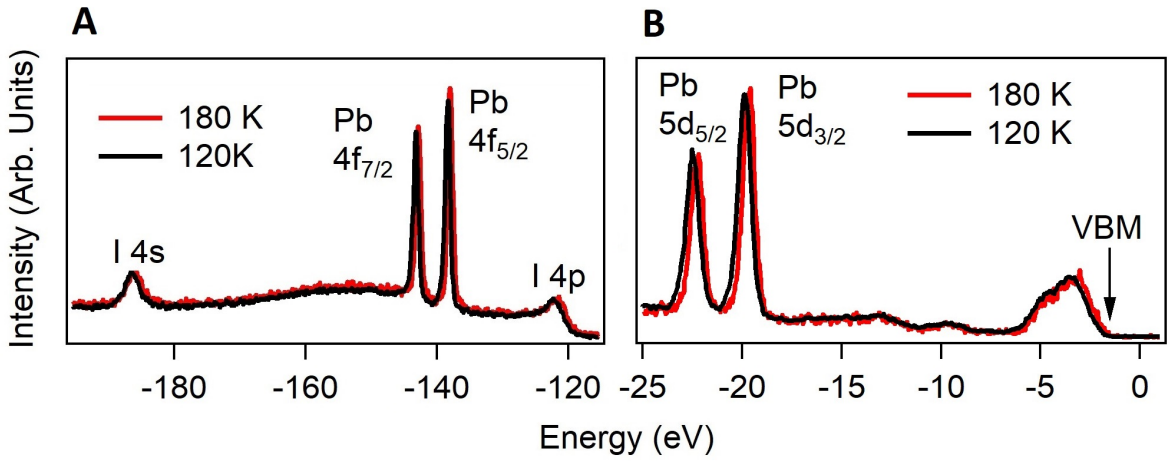

Figure 1: A: Hard X-ray photoelectron spectrum of $CH_3NH_3PbI_3$ showing the I $4s$, Pb $4f$, I $4p$ levels in the tetragonal phase at 180 K (red line) and in the orthorhombic phase at 120 K (black line). B: Photoelectron spectrum of $CH_3NH_3PbI_3$ showing the valence band and Pb $5d$ levels in the tetragonal and orthorhombic phases. The data have been acquired with photon energy of 3000 eV.

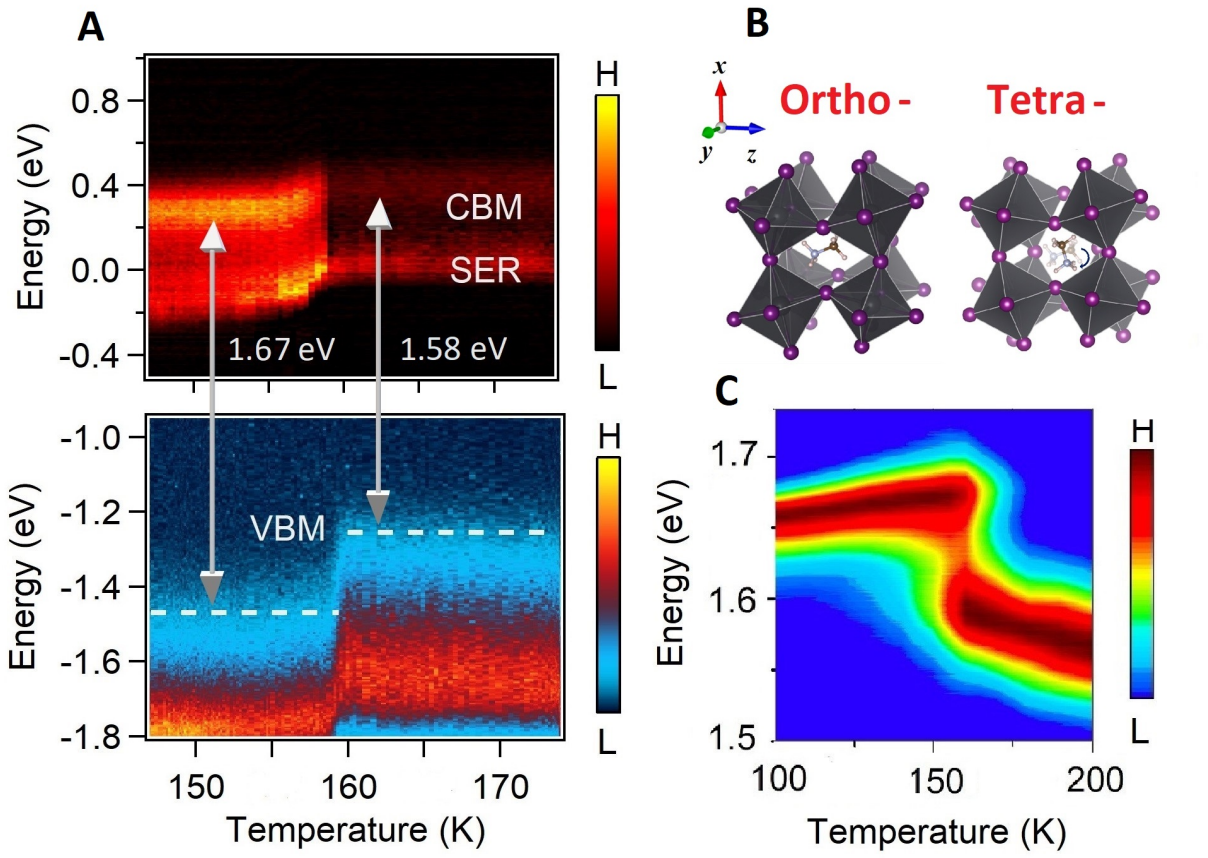

Figure 2: A: Photoelectron intensity map of $CH_3NH_3PbI_3$ collected at pump probe delay of 1.5 ps and as a function of temperature. The upper panel is acquired with probe photon energy of 4.7 eV. It shows a peak corresponding to the Conduction Band Minimum (CBM) and Secondary Electrons Replica (SER, which coincides with the spectral cutoff at zero kinetic energy). The lower panel is acquired with a probe photon energy of 6.3 eV, leading to a photoelectron intensity that vanishes at the Valence Band Maximum (VBM, indicated by a dashed white line). The origin of the energy axis corresponds to the position of the chemical potential, both in the lower and upper panel. Grey arrows stand for the bandgap size below and above the phase transition. B: Sketch of a crystal structure in the tetragonal and orthorhombic phase. C: Photoluminescence intensity map as a function of temperature.

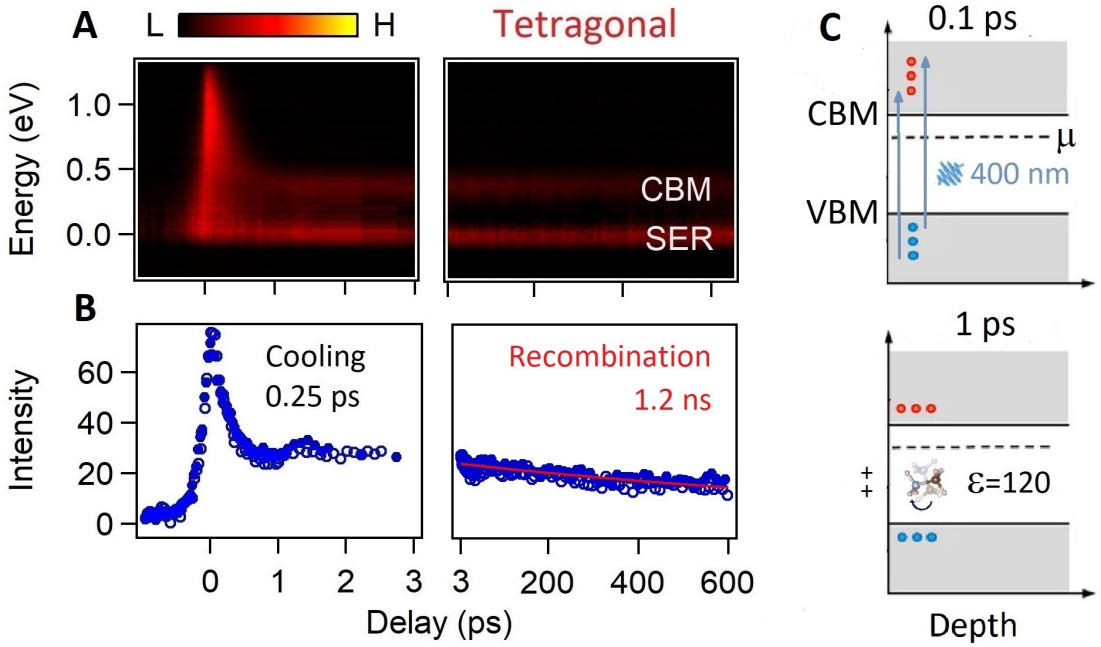

Figure 3: A: Photoelectron intensity map of $CH_3NH_3PbI_3$ acquired in the tetragonal phase at 180 K as a function of pump probe delay. The Conduction Band Minimum (CBM) and Secondary Electrons Replica (SER) are indicated on the plot. B: Photoelectron intensity integrated in a energy interval of 0.1 eV around the CBM as a function of pump probe delay (T=180 K). Open and filled circles correspond to two subsequent scans. The excellent reproducibility of the data excludes that exposure of the probe or pump beam induces any surface degradation. The cooling and recombination time of hot carriers is 0.25 ps and 1.2 ns, respectively. C: Sketch of carriers relaxation at the highly screened surface of the tetragonal phase ($\varepsilon = 120$).

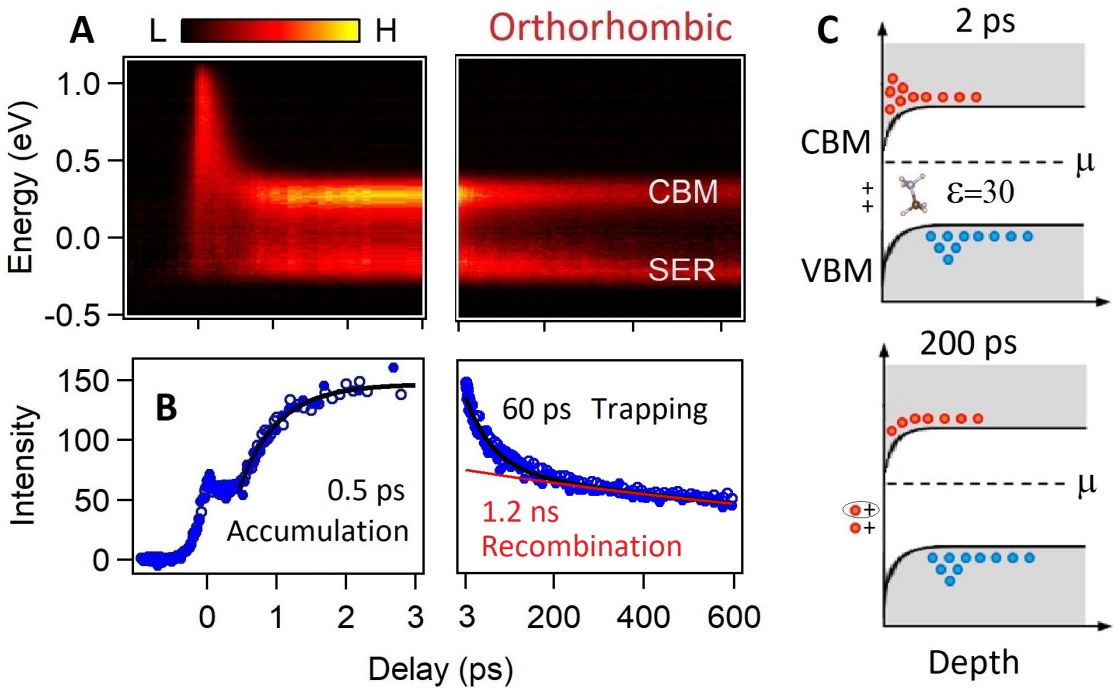

Figure 4: A: Photoelectron intensity map of $CH_3NH_3PbI_3$ acquired in the Orthorhombic phase at 140 K as a function of pump probe delay. The Conduction Band Minimum (CBM) and Secondary Electrons Replica (SER) are indicated on the plot. B: Photoelectron intensity integrated in a energy interval of 0.1 eV around the CBM as a function of pump probe delay (T=140 K). Open and filled circles correspond to two subsequent scans. The accumulation of electrons at the surface saturates after 2-3 ps and displays build up constant of 0.5 ps. Subsequently the electronic density in the CBM decays because of trapping (dark line, 60 ps) and recombination (red line, 1.2 ns). C: Sketch of electrons accumulation at the poorly screened surface termination of the orthorhombic phase ($\varepsilon = 30$) and (lower panel) subsequent trapping of electrons in vacancies or interstitial defects at the surface.

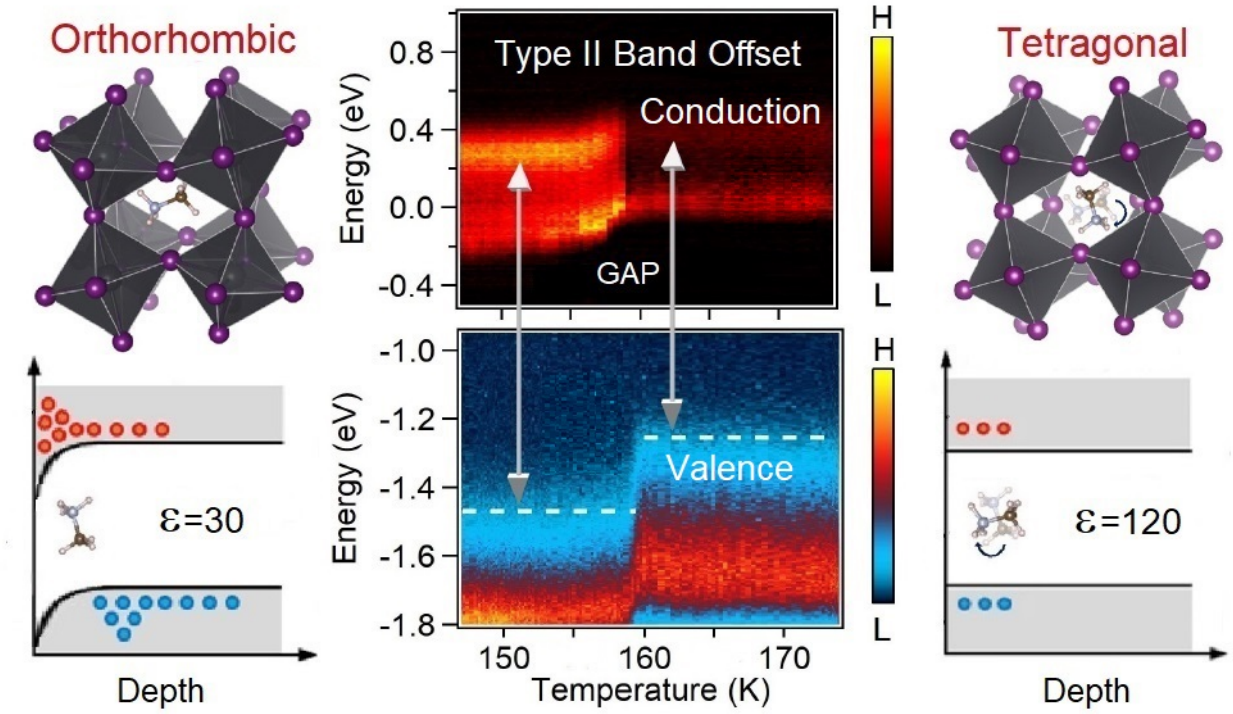

Figure 5: TOC graphics